Liquation Tendency and Liquid-Film Formation in Friction Stir Spot Welding

The tendency is ranked among different alloys and explained, and the evidence of liquid-film formation and its effect on the resultant weld are presented

BY Y. K. YANG, H. DONG, AND S. KOU

ABSTRACT. Friction stir spot welding (FSSW) is considered to be solid-state welding, but recent studies have shown that liquation (i.e., liquid formation) can occur in FSSW of some Al and Mg alloys such as 2024 Al, 7075 Al, and AZ91 Mg. Instead of these more complicated multicomponent alloys, a simple binary alloy with an easy-to-understand microstructure, that is, 2219 Al (~Al-6.5Cu), was used to study liquation in FSSW and its effect on the resultant weld. The first part of the study focused on assessing the liquation tendency of 2219 Al. An augmented-torque test was used, and the extent of liquation in 2219 Al was compared with those in 6061 Al and AZ91E Mg. The liquation tendency increased in the order of 6061 Al, 2219 Al, and AZ91E Mg. The torque measured during FSSW showed that the heat input decreased in the same order. The liquation tendency was explained by using a method based on both the phase diagram and the curves of temperature vs. fraction solid during solidification, which indicated that the amount of liquation-inducing constituent increased and the liquation temperature decreased in the same order. The second part focused on examining liquation in 2219 Al. The amount of material stuck to and removed by the tool increased with increasing tool rotation speed. The evidence of liquid-film formation observed included 1) a thin eutectic film at the interface between the weld and the residue of the material removed, 2) thin eutectic films in the stir zone, 3) a mirror-like weld surface or fracture surface, and 4) a high concentration of eutectic particles in the stir zone at a location corresponding to the fracture surface. In addition to material removal by the tool, liquation during FSSW caused erosion or fracture at the weld surface and cracking in the stir zone.

Y. K. YANG and S. KOU are, respectively, graduate student and professor in the Department of Materials Science and Engineering, University of Wisconsin, Madison, Wis. H. DONG is lecturer, School of Materials Science and Engineering, Dalian University of Technology, Dalian, China.

Introduction

Friction stir welding (FSW) was invented by The Welding Institute (Ref. 1). A rotating cylindrical tool with a pin at its bottom is first plunged into a rigidly held workpiece and then traversed along the joint to achieve welding by plastic flow of frictionally heated material from ahead of the pin to behind it. High plasticity of the material in FSW has been attributed to the very fine grains produced by dynamic recrystallization caused by the intense plastic deformation associated with the movement of material around the pin and friction heating (Refs. 2, 3). Friction stir spot welding (FSSW) is similar, but without traversing the tool. As shown in Fig. 1, the rotating tool is first plunged into the workpiece, allowed to stir up the adjacent material at the joint surface, and then withdrawn from the workpiece. Spot welding is achieved by plastic flow of frictionally heated material around the pin. A keyhole is left in the workpiece after the tool is withdrawn.

In FSW, the tool travels along the joint and the heat input is distributed along the joint. Liquation, that is, formation of liquid, rarely occurs in FSW. Cao and Kou (Ref. 4) found no liquation in FSW of 2219 Al. However, in FSSW the tool remains at one spot, where the heat input dwells. Thus, liquation is much more likely to occur.

Temperature measurements have been conducted in FSSW by Gerlich, Yamamoto, North, and coworkers (Refs. 5–9) with thermocouples embedded in a stationary alloy-steel tool to measure temperatures in a rotating workpiece at the surfaces of the tool shoulder and pin. Temperatures approaching or exceeding the liquation temperature have been measured during the FSSW of some Al and Mg alloys, and microstructural evidence of liquation has been observed (Refs. 5–9). Gerlich (Ref. 9) determined the strain rate of the material adjacent to the rotating tool based on electron backscattered diffraction (EBSD). In both 2024 Al and 7075 Al, the stain rate dropped sharply above a high rotation speed, e.g., 1500 rev/min. This was attributed to tool slippage caused by liquation.

Yang et al. (Ref. 10) have investigated liquation in FSSW of Mg alloys. They demonstrated: 1) a liquation-susceptibility test with an augmented torque during FSSW to amplify the difference in the extents of liquation between different alloys, and 2) a method to explain the liquation susceptibility based on the phase diagram and the curve of temperature vs. fraction solid (T-f_S) during solidification.

Kou and coworkers (Refs. 11–17) have shown liquation-induced cracking in the partially melted zone (PMZ) of Al arc welds and the severe loss of ductility and strength of the PMZ even in the absence of cracking. Various liquation mechanisms in Al arc welds have been discussed by Kou (Ref. 18).

The purpose of the present study is to investigate liquation in FSSW using a simple binary alloy that has a well-documented phase diagram and easy-to-understand microstructure, that is, 2219 Al (~Al-6.5Cu), instead of the more complicated multicomponent alloys studied so far such as 2024 Al, 7075 Al, and AZ91 Mg. The study consists of two parts. First, 2219 Al is compared with 6061 Al and AZ91E Mg in the tendency to liquate using the augmented-torque test of Yang et al. (Ref. 10), and the results are explained using the method of Yang et al. (Ref. 10) based on the phase diagram and the T-f_S curve. Second, liquation in 2219

KEYWORDS

Friction Stir Spot Welding
Friction Stir Welding
Liquation
Liquation Cracking
2219 Aluminum
6061 Aluminum
AZ91 Magnesium

Al is examined, including the evidence of liquid-film formation and its effect on the resultant weld.

Experimental Procedure

The workpiece was 2219-T851 Al. "T8" stands for solution heat treating and cold working, followed by artificial aging, and Tx51 stands for stress relieving by stretching (Ref. 19). The actual composition of the alloy is listed in Table 1. The workpiece was either one single piece of 9.5-mm- (⅜-in.-) thick 2219 Al or two pieces of 2219 Al milled down from 9.5mm to about 4.6 mm and stacked up to an overall thickness of about 9.2 mm. All pieces were 55 by 55 mm (2⅛ by 2⅛ in.) in size. The workpiece was welded in the T851 condition.

As in the augmented-torque test of Yang et al. (Ref. 10), the tool for all FSSW experiments was a H13-steel tool with a shoulder of 15 mm diameter and a threaded pin of 5.5 mm diameter and 5.1 mm length beyond the bottom of the shoulder. Figure 2 shows the tool. It was originally designed by Friction Stir Link, Inc., Menomonee Falls, Wis., for FSW of 6-mm-thick Al alloys. Two different milling machines were used for FSSW. Initially, a Lagun FTV-1 milling machine (2.2 kW or 3 hp) was used. Later, a HAAS TM1 CNC milling machine (5.5 kW or 7.5 hp) was adopted. The tool rotation speed ranged from 1000 to 3000 rev/min, counterclockwise when viewed from above. The plunge rate was about 0.15 mm/s and the dwell time 4 s. The plunge rate was kept low to prevent the tool from stalling during FSSW with the Lagun milling machine. After each weld was made, the tool was plunged into a piece of Alloy 6061 to clean off the Alloy 2219 stuck to the tool during welding. Unlike 2219 Al, 6061 Al did not stick to the tool after welding possibly because it is more extrudable and less likely to liquate.

The measurement of the torque and axial force during FSSW was similar to that described by Yang et al. (Ref. 10). A Kistler Type 9271A dynamometer was mounted on the HAAS TM1 CNC milling machine. The dynamometer was cylindrical in shape, and it allowed both the moment acting about its axis and the force parallel to its axis to be measured during FSSW. The dynamometer allowed torque measurements in the range of –100 to +100 Nm with a 0.02-Ncm threshold and –1.5 pC/Ncm sensitivity for the torque and force measurements in the range of –5 to +20 kN with a 0.02-N threshold and –1.8 pC/N sensitivity for the axial force. A computer-based data acquisition system was used to collect the data at 250 Hz and display in real time the curves of torque vs. time and axial force vs. time.

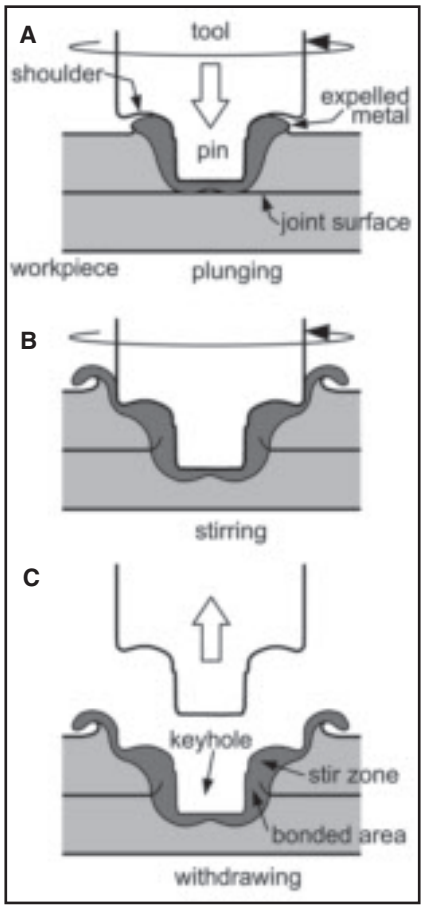

Fig. 1 — Friction stir spot welding (FSSW). A — Plunging; B — stirring; C — withdrawing.

The resultant 2219 Al welds were cut along the rolling direction of the workpiece, polished, and etched with a solution of 0.5 vol-% HF in water for microstructural examination by optical microscopy and scanning electron microscopy (SEM) in the secondary electron mode at 15 kV and a 15-mm working distance. The composition of the intermetallic compound or eutectic particles in the alloy was determined by energy-dispersive spectroscopy (EDS) to help identify them. Photos of the cross sections of the welds were taken with a digital camera.

Results and Discussion

Liquation Tendency in FSSW

Figure 3 shows the top surfaces of the welds after FSSW with the HAAS TM1 CNC milling machine at 1000 rev/min. The welds of 6061-T6 Al and as-cast AZ91E Mg were made in a previous study (Ref. 10). In the case of 6061 Al (Fig. 3A), the top surface of the weld shows no evidence of any erosion, fracture, or liquid formation. There is no microstructural evidence of liquation or cracking in the stir zone as already confirmed previously (Ref. 10). In the case of 2219 Al (Fig. 3B), however, the top surface of the weld is missing in the area indicated by the broken line. As will be shown subsequently (in Fig. 7B), there is some cracking in the stir zone. As for AZ91E Mg (Fig. 3C), the entire top surface of the weld is mirror like, suggesting severe liquid formation. Liquation and cracking are both severe in the stir zone as already shown previously by the stir-zone microstructure (Ref. 10). Thus, the liquation tendency in FSSW increases in the order of 6061 Al, 2219 Al, and AZ91E Mg.

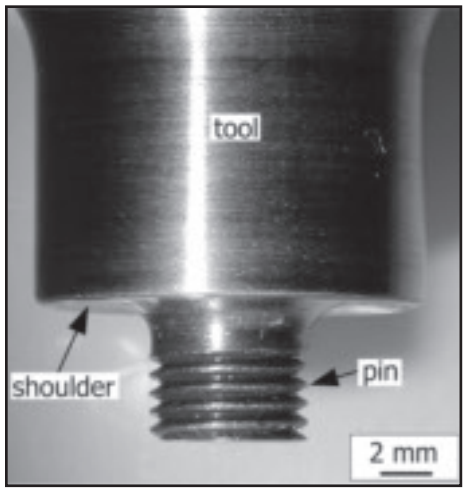

Fig. 2 — Tool with a 15-mm-diameter shoulder for FSSW with augmented torque.

Torque and Axial Force

Figure 4 shows the torque M_z and axial F_z of the rotating tool measured during FSSW of the welds mentioned in Fig. 3. The data for 6061-T6 Al and as-cast AZ91E Mg were obtained previously

Table 1 — Compositions of Workpiece Materials (wt-%)

	Si	Cu	Mn	Mg	Cr	Zn	Ti	Fe	Zr	Al
2219 Al	0.09	6.49	0.32	0.01	—	0.03	0.06	0.14	0.13	bal.
6061 Al	0.62	0.28	0.08	0.89	0.19	0.02	0.01	0.52	—	bal.
AZ91E Mg	—	—	0.24	bal.	—	0.65	—	—	—	8.60

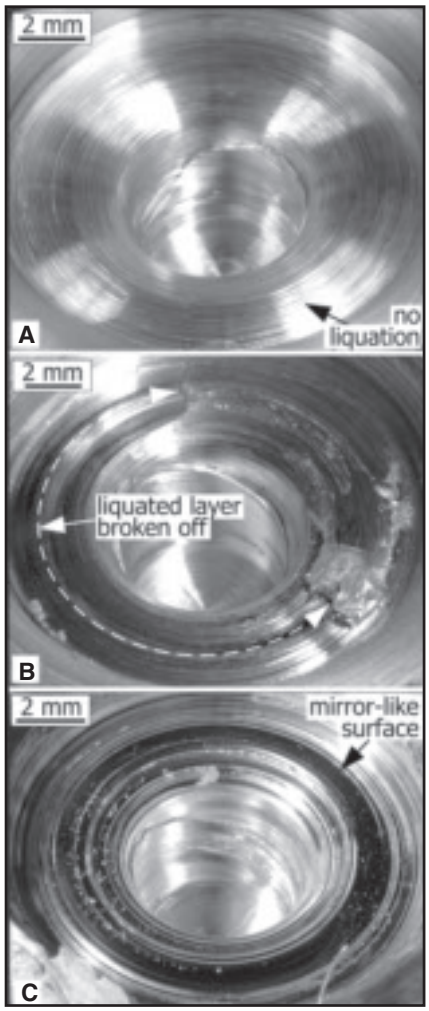

Fig. 3 — Top surfaces of welds showing the following: A — No evidence of liquation in 6061 Al; B — liquated layer broken off from 2219 Al in the area indicated by the broken line; C — mirror-like liquated surface of AZ91E Mg. 1000 rev/min rotation speed. A and C from Yang et al. (Ref. 10).

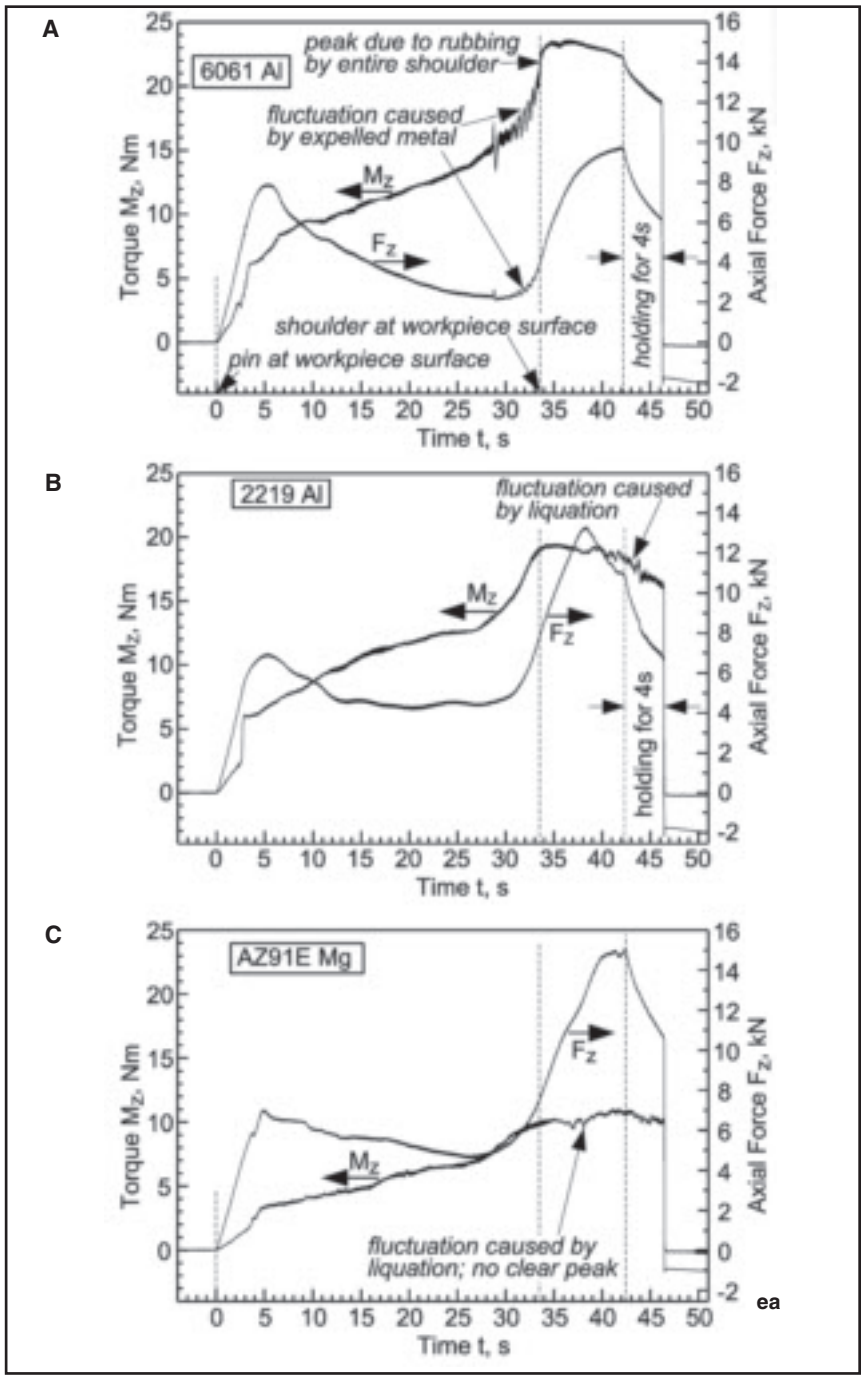

Fig. 4 — Tool torque and axial force measured during FSSW. A — 6061 Al; B — 2219 Al; C — AZ91E Mg. Area under each curve proportional to heat input generated by either rotation (M_Z) or plunge (F_Z) of tool. 1000 rev/min rotation speed. A and C from Yang et al. (Ref. 10).

under an identical FSSW schedule (Ref. 10). Both the torque and the axial force vary with time and from alloy to alloy. For 6061 Al (Fig. 4A), the torque rose quickly initially and then more slowly as the adjacent workpiece material is heated up and softened by the friction heat produced. It increases steadily as the tool penetrates deeper into the workpiece. As the shoulder approaches the workpiece surface, the torque rose sharply to a peak of about 23 Nm. The curve of the axial force F_z vs. time t shows two peaks, one shortly after the beginning of welding and the other toward the end. The axial force rose quickly initially but decreased as the adjacent workpiece material heated up and softened. This results in the first peak. The axial force rose quickly again as the tool shoulder approached the workpiece surface. Both the torque and the axial force fluctuated shortly before the tool shoulder reached the workpiece surface. This was likely caused by the material expelled by the tool but entrapped between the rotating shoulder and the stationary workpiece surface, which tended to switch back and forth between rotating and stopping.

For 2219 Al (Fig. 4B), the torque curve was similar to that of 6061 Al. However, the peak torque was only about 19 Nm, significantly lower than the 23-Nm peak torque in the case of 6061 Al. Furthermore, the torque fluctuated significantly toward the end of welding. For AZ91E Mg (Fig. 4C), the torque curve was far below those of 6061 Al and 2219 Al, with a peak torque of only about 11 Nm. The torque also fluctuated significantly toward the end of welding.

The torque fluctuations observed in 2219 Al (Fig. 4B) and AZ91E Mg (Fig. 4C) are likely to be caused by liquation. It

Table 2 — Heat inputs in FSSW

	Heat Input from Rotation Q_Ω (J)	Heat Input from Plunging Q_F (J)	Total Heat Input Q (J)	Area $\int$ Mz dt (Nm s)	Area $\int$ Fz dt (kN s)
6061 Al	67512	35	67547	644.7	232.9
2219 Al	61062	45	61107	583.1	298.2
AZ91E Mg	32285	51	32336	308.3	338.3

is likely that when liquid forms, the torque and hence temperature tend to decrease. When the liquid cools and solidifies, the torque and hence temperature tend to increase, and liquid forms again to repeat the cycle. When welding 2219 Al at higher rotation speeds (e.g., 2000 rev/min), the authors observed sudden appearance of powder at the workpiece surface around the rotating tool, and the powder seemed somewhat wet (i.e., liquated). The vertical cross sections of the resultant welds showed removal of a significant amount of stir-zone material by the tool. It appeared that the pieces of solid broken off suddenly from the liquated region were caught, dragged, and ground by the rotating tool shoulder. This action could have also contributed to the torque fluctuation.

Heat Input during FSSW

The rotation-induced heat input Q_Ω (in Joules) is as follows (Ref. 20):

$$Q_\Omega = \int_0^t M_z \left(\frac{2\pi\Omega}{60}\right) dt \qquad (1)$$

where M_z is the torque (in Nm), Ω the rotation speed (in rev/min), and t time (in s). Likewise, the plunge-induced heat input Q_F (in Joules) is as follows:

$$Q_F = \int_0^t F_z v_z dt \qquad (2)$$

where F_z is the axial force (in N) and v_z the plunge rate (in m/s). Both the rotation speed Ω and the plunge rate v_z are often held constant during FSSW. For all three materials in the present study, Ω (= 1000 rev/min) and v_z (= 1.5×10^{-4} m/s) are both constant. Thus, for constant Ω and v_z, the total heat input Q due to both tool rotation and plunge in FSSW is as follows:

$$Q = Q_\Omega + Q_F = \left(\frac{2\pi\Omega}{60}\right)\int_0^t M_z \, dt + v_z \int_0^t F_z dt \quad (3)$$

The first integral on the right-hand side of Equation 3 is the area under the curve of torque vs. time. This area is highest with 6061 Al, slightly (about 10%) lower with 2219 Al, and much lower (about 50%) with AZ91 Mg. Likewise, the second integral on the right-hand side of Equation 3 is the area under the curve of axial force F_z vs. time t. This area is lowest with 6061 Al, significantly (about 30%) higher with 2219 Al, and even higher (45%) with AZ91 Mg. The heat input Q_F due to tool plunge tends to be much smaller than the heat input Q_Ω due to tool rotation. Table 2 lists the heat inputs during the FSSW of the three different materials, the total heat input Q is highest with 6061 Al (67,547 Joules), slightly lower with 2219 Al (61,107 Joules), and much lower with AZ91E Mg (32,336 Joules).

Thus, the increasing extent of liquation in the order of 6061 Al, 2219 Al, and AZ91E Mg (Fig. 3) could not have been caused by an increasing heat input in the same order.

Explanation for Liquation Tendency in FSSW

The fact that the increasing liquation tendency in the order of 6061 Al, 2219 Al, and AZ91E Mg cannot be explained by the heat input suggests that the tendency is related to the alloys themselves. As mentioned previously, Yang et al. (Ref. 10) explained the tendency of an alloy to liquate in FSSW based on the phase diagram and the curve of temperature vs. fraction solid (T-f_S) during solidification. The phase diagram and the T-f_S curve together can help identify the liquation-causing constituent in the alloy, for instance, an intermetallic compound in a wrought alloy or a eutectic in an as-cast alloy. In some cases, they can also help estimate the amount of the liquation-causing constituent. In any case, the more abundant the liquation-causing constituent and the lower the liquation temperature, the greater the liquation tendency tends to be.

Figure 5 shows the T-f_S curves of 6061 Al, 2219 Al, and AZ91E Mg. They were calculated based on the Scheil model using the multicomponent solidification software Pandat (Ref. 21) and the data base PanAluminum (Ref. 22). The T-f_S curve for AZ91E Mg was calculated by

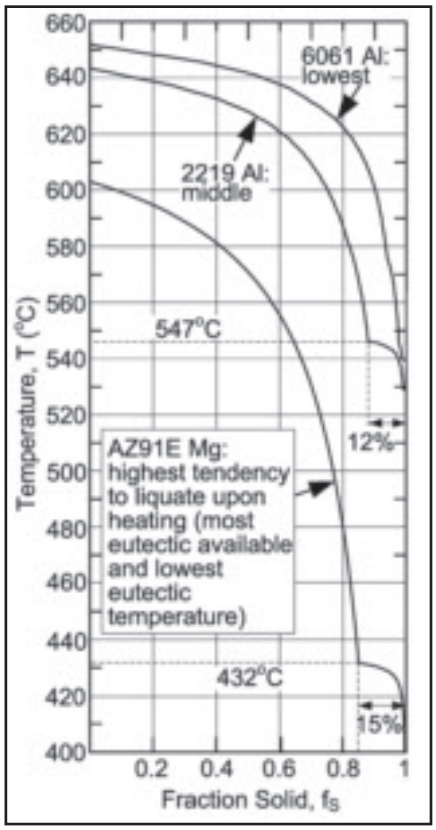

Fig. 5 — Curves of temperature (T) vs. fraction solid (f_S) for 6061 Al, 2219 Al, and AZ91E Mg alloys during solidification. Curves calculated based on Scheil model of multicomponent alloys using Pandat of CompuTherm LLC (Ref. 21). Curve for AZ91 Mg taken from Ohno et al. (Ref. 23).

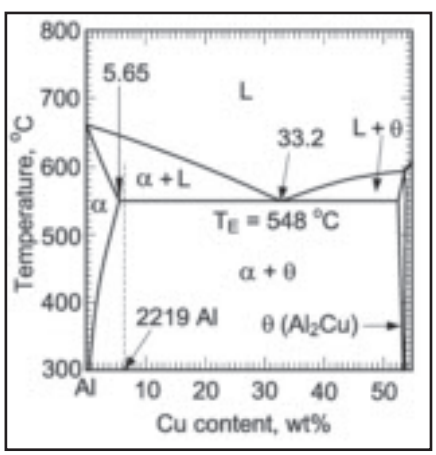

Fig. 6 — Aluminum-rich side of Al-Cu phase diagram (Ref. 24).

Ohno et al. (Ref. 23) also using Pandat. As shown by its T-f_S curve, 6061 Al does not have much liquation-causing constituent present even in the as-cast condition. Even less or none is left after the T6 heat treating.

The Al-Cu phase diagram (Ref. 24) in Fig. 6 shows that 2219 Al, which is essentially an Al-6.5Cu binary alloy, consists of

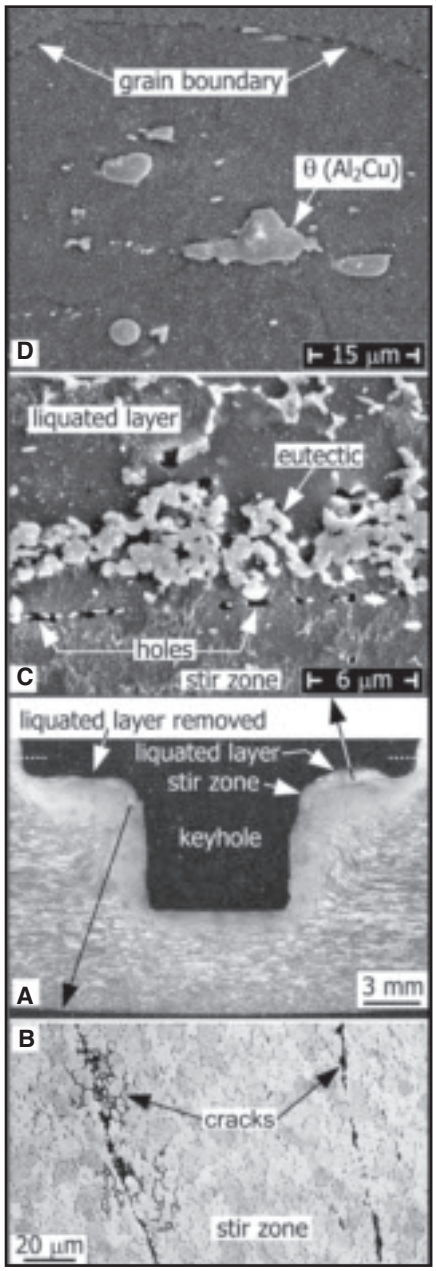

Fig. 7 — Liquation in 2219 Al. A — Vertical cross section; B — cracks near keyhole; C — SEM image showing eutectic in liquated layer; D — SEM image showing base-metal microstructure. 1000 rev/min rotation speed.

an Al-rich matrix α and θ (Al_2Cu) particles in it. Plenty of θ particles are always present in 2219 Al because the 6.5 wt-% Cu content of 2219 Al is beyond the 5.65 wt-% Cu solubility limit of the Al-rich, α phase. The composition of the θ particles is about Al-53.5Cu (by wt-%). The eutectic temperature T_E is 548°C. Upon heating to T_E during welding, liquation occurs by the eutectic reaction $\alpha + \theta \rightarrow L$. Liquation occurs at T_E regardless of the heating rate during welding. Obviously, this is not the "constitutional liquation" mechanism proposed by Pepe and Savage (Refs. 25, 26), which requires fast heating during welding in order to allow θ particles to remain until T_E is reached to cause liquation. Upon cooling, the eutectic liquid L solidifies into either a normal composite-like eutectic (α + θ) or a divorced eutectic, that is, θ particles surrounded by α grown from the α matrix.

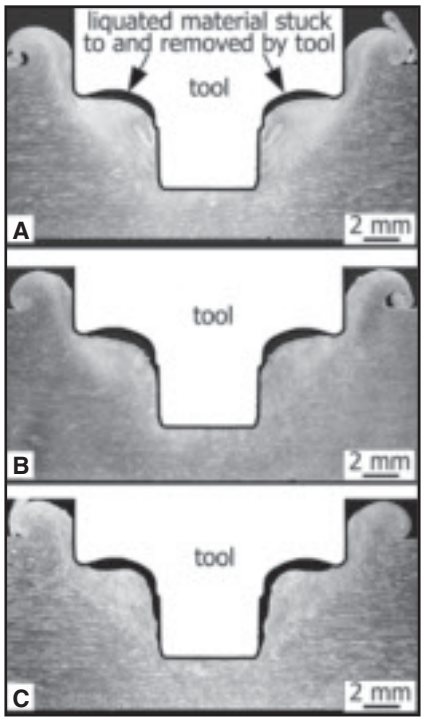

Fig. 8 — Increasing removal of liquated material from 2219 Al by tool with increasing tool rotation speed. A — 1500 rev/min; B — 2000 rev/min; C — 3000 rev/min. The area of gap between tool and weld represents material removed.

As-cast 2219 Al, as shown by its T-f_S curve in Fig. 5, has about 12% eutectic to cause liquation, much more than 6061 Al. Based on Al-6.5Cu as a composition approximation and the binary Al-Cu phase diagram (Fig. 6), 2219 Al cannot be heat treated after casting to an Al-rich phase (α phase) without θ (Al_2Cu) particles because its Cu content is beyond the solute solubility of 5.65% dictated by the phase diagram. That is, the liquation-causing constituent θ (Al_2Cu) cannot be dissolved away by heat treating. Thus, 2219-T851 Al can be expected to have a greater tendency to liquate than 6061-T6 Al, as has been observed in arc welding (Ref. 12). As mentioned previously, after each welding experiment of 2219-T851 Al, the material stuck to the tool because of liquation was cleaned off by plunging the tool into a separate piece of 6061-T6 Al. No sticking of 6061-T6 to the tool was observed in the present study.

According to its T-f_S curve shown in Fig. 5, the as-cast AZ91E Mg has a rather high fraction of eutectic of about 15% and a very low eutectic temperature of 432°C, which is 115°C lower than the eutectic temperature of 2219 Al 547°C. This clearly suggests that as-cast AZ91E Mg should have a significantly greater tendency to liquate than 2219-T851 Al. The mirror-like weld surface with circular grooves (Fig. 3C) and the severe liquation and cracking in the stir zone (Ref. 10) all confirm the high liquation tendency of AZ91E Mg.

Liquation in 2219 Al

Evidence of liquation was observed, including a liquated layer at the weld top surface and cracks in the stir zone near the keyhole. Figure 7 is the 2219-T851 Al weld mentioned previously in Figs. 3B and 4B. Figure 7A shows the vertical cross section of the weld. The top surface of the weld is lower on the left-hand side than the right-hand side. That is, the layer of liquated material on the left-hand side in contact with the tool shoulder during welding was removed by the tool.

The stir-zone microstructure in Fig. 7B shows cracks roughly parallel to the vertical wall of the keyhole. The light-etching band at the mid-height of the micrograph in Fig. 7C is a layer of eutectic. It is likely that there was a higher concentration of θ (Al_2Cu) particles here, and they reacted with the surrounding α matrix to form liquid eutectic. Upon cooling, the liquid eutectic solidified into solid eutectic. A horizontal series of small holes exists at the bottom of the eutectic layer, indicating the interface between the liquated layer on the top and the stir zone below it. Further to the right and beyond the micrograph in Fig. 7C, the holes are connected to each other into a continuous gap. The base-metal microstructure far away from the keyhole is shown by the SEM image in Fig. 7D. EDS showed that the particles are Cu rich, suggesting they are the θ (Al_2Cu) particles typically found in 2219 Al.

Effect of Tool Rotation Speed on Material Removal

The amount of material stuck to and removed by the tool (when the tool was withdrawn at the end of FSSW) increased with increasing tool rotation speed because more friction heat is generated by faster tool rotation to fuel liquation. Figure 8 shows welds made with the HAAS milling machine at different rotation speeds, with a nearly constant tool penetration of 6.5 to 6.8 mm from the pin tip to the workpiece surface. A gap existed between the tool and the surface of each weld. The area of the gap represented the amount of material removed by the tool.

As the rotation speed increased, the re-

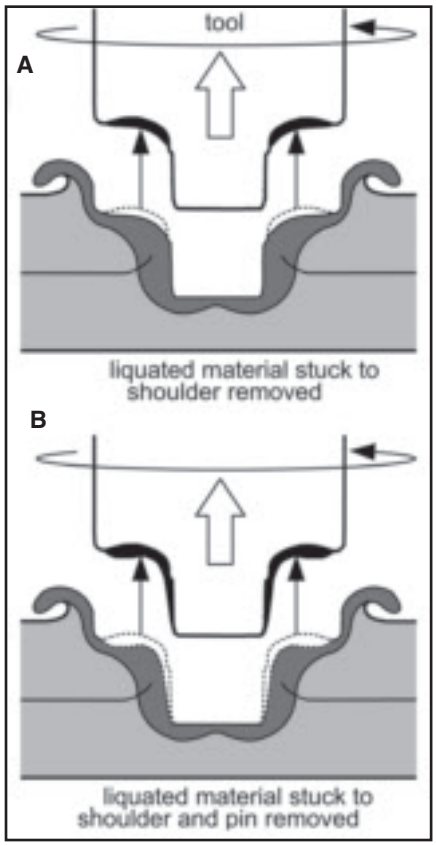

Fig. 9 — Liquated material stuck to and removed by tool at end of FSSW. A — From near shoulder; B — from near shoulder and pin — bonding reduced.

moval of material extended downward from near the shoulder to around the pin and made the resultant keyhole more like a truncated cone. However, the material in contact with the outer edge of the shoulder did not stick to and leave with the tool when the tool was withdrawn at the end of welding.

The material removed from around the pin can reduce the joint strength of the resultant weld. As shown in Fig. 9, when the material around the pin is removed, the thickness of the bonding area is reduced. If the thickness reduced is significant as compared to the thickness of the bonding area, the strength of the resultant weld can decrease significantly. Thus, for a workpiece that needs a high rotation speed to plasticize the material around the pin to achieve bonding, it is desirable to check if it also has a strong tendency to liquate upon heating.

Mirror-Like Weld Surface

The weld from which a significant amount of material was removed by the tool tended to have a mirror-like surface. Figure 10A shows the vertical cross section of the weld made with the HAAS milling machine at 3000 rev/min (Fig. 8C). The weld surface was mirror like as shown in Fig. 10B. The mirror-like weld surface suggests the following: 1) During welding a thin liquid film was present at the interface between the material removed by the tool and the material left behind as the weld, and 2) the film promoted easy removal of the liquated material by the tool.

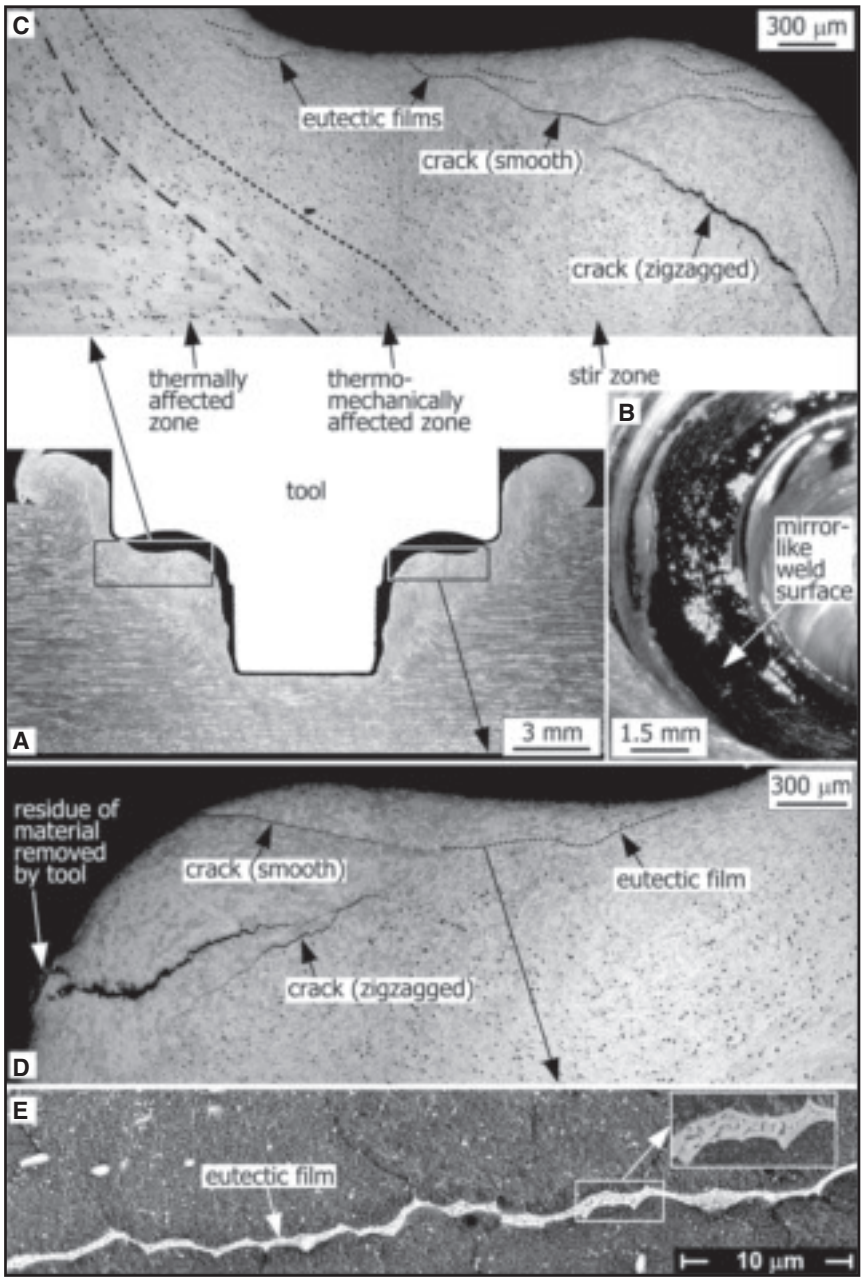

Fig. 10 — Microstructure below a mirror-like weld surface. A — Vertical cross section; B — mirror-like weld surface; C and D — cracks and eutectic films in stir zone; E — SEM image of eutectic film.

Cracks and Eutectic Films in Stir Zone

Cracks were found in the stir zone of the weld with a mirror-like surface. As shown by the optical micrographs in Fig. 10C and D, both smooth and zigzagged cracks were present in the stir zone, but the former is closer to the weld surface. Both cracks are intergranular. Zigzagged cracking is typical of liquation cracking in arc welds. The micrographs were taken with the sample only lightly etched in order to help bring out the cracks and θ (Al_2Cu) particles (which appeared as dark dots) more clearly. This is why the micrographs do not show the grain structure very clearly. However, the grain structure

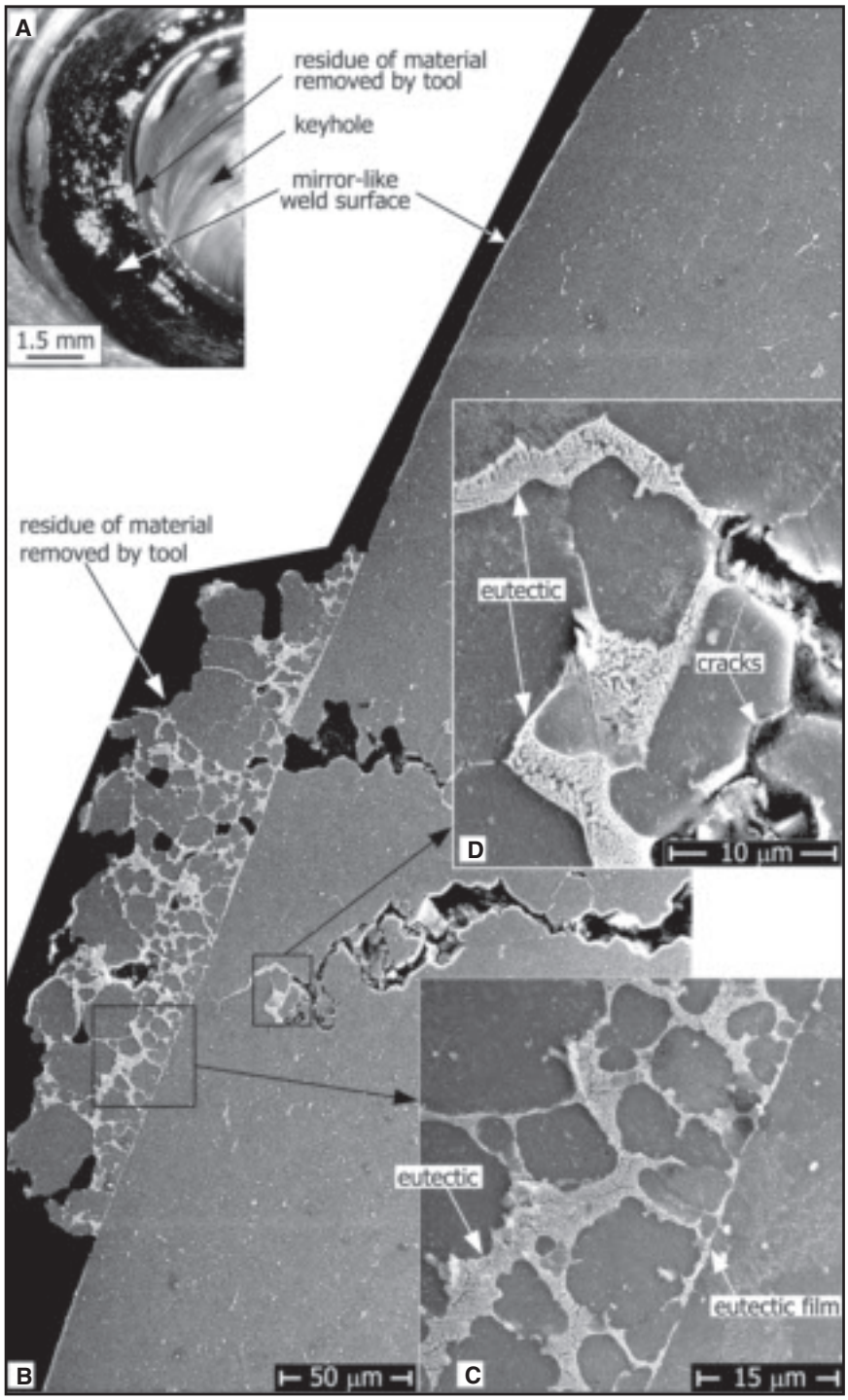

Fig. 11 — Microstructure near a mirror-like weld surface. A — Mirror-like weld surface with some residue on it; B — SEM image showing the vertical cross section of the weld surface and the residue on it; C — SEM image showing eutectic in film and residue; D — SEM image showing cracks.

has already been shown in Fig. 10A, where the coarse elongated grains in the base metal are clearly visible but the grains in the stir zone are too fine to see.

Examination of the same weld sample at higher magnifications revealed a number of eutectic films scattered in the stir zone. These eutectic films are shown as dashed lines in Fig. 10C and D because they are too thin to be visible at the magnification level of the optical micrographs. As shown, the smooth cracks were connected to eutectic films. This clearly indicates that the smooth cracks were in fact eutectic liquid films before cracking occurred. Cracks along eutectic liquid films suggest cracking induced by liquation during FSSW.

Figure 10E is a SEM image showing a eutectic film in Fig. 10D, with the composite-like eutectic structure enlarged in the inset. As shown, the eutectic film is very thin, only on the order of 1 μm, and it is essentially smooth instead of highly zigzagged. Because the liquid films were very thin in the first place, little eutectic could be observed along the open cracks. Thus, the liquid-film formation is difficult to confirm if there are only open cracks in the weld and no eutectic films. Alloys that form a significant amount of eutectic upon liquation provide a better chance for liquid films to be found in the resultant weld. AZ91 Mg, 2024 Al, 2219 Al, and 7075 Al are examples of such alloys. However, only 2219 Al is a binary alloy (essentially Al-6.5Cu) and was thus selected for the present study. Furthermore, the Cu content of Alloy 2219 (6.5 wt-% Cu) is beyond the maximum solid solubility of Cu in the Al-rich matrix α (5.65 wt-% Cu). Consequently, not all the eutectic produced by liquation can be dissolved in the matrix α even if the peak temperature there during FSSW exceeds the eutectic temperature.

Perhaps, one possible mechanism for cracking to occur well within the stir zone and near its surface, such as that shown in Fig. 10C and D, is cracking of a semisolid in the two-phase (α + L) region of the phase diagram. This mechanism differs from the liquid-penetration-induced (LPI) cracking mechanism proposed by Yamamoto et al. (Ref. 6), which explains cracking in the stir zone near its boundary with the base metal. It is likely that the eutectic temperature T_E was exceeded slightly in the stir zone near the weld surface, where θ (Al_2Cu) particles (dark dots in Fig. 10C and D) disappeared and eutectic films and smooth cracks existed. In other words, the material here might have already entered the two-phase region of (α + L) in the phase diagram shown in Fig. 6, causing the θ (Al_2Cu) particles to disappear and a semisolid to form. Under the torque of the rotating tool, the semisolid can crack smoothly near the weld surface where the temperature and hence the fraction of liquid are higher. Upon cooling, the liquid along the crack can solidify and become eutectic at the eutectic temperature. Farther away from the weld surface where the temperature and hence the fraction of liquid are lower, the semisolid can crack intergranularly (in a zigzagged fashion).

Eutectic Film under Liquated Material

A eutectic film was found between the

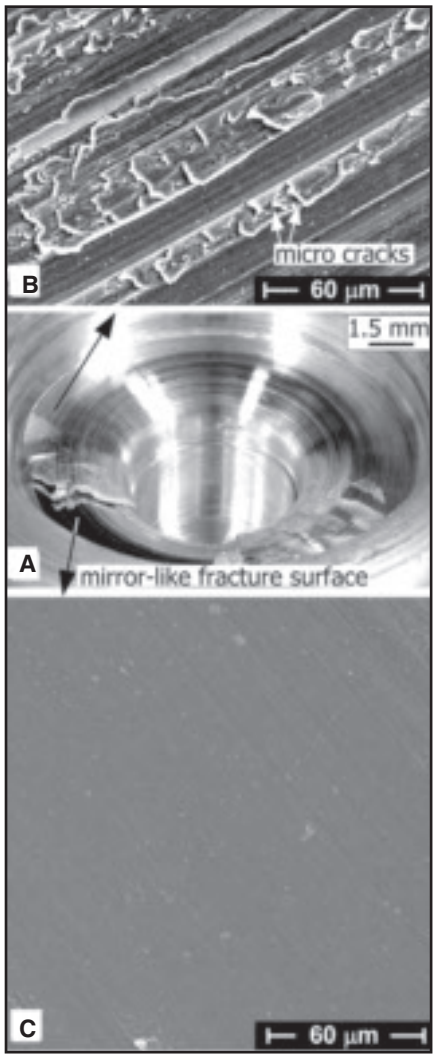

Fig. 12 — Mirror-like fracture surface. A — Overview; B — SEM image showing tool-shoulder tracks on weld surface; C — SEM image showing smoothness of mirror-like fracture surface.

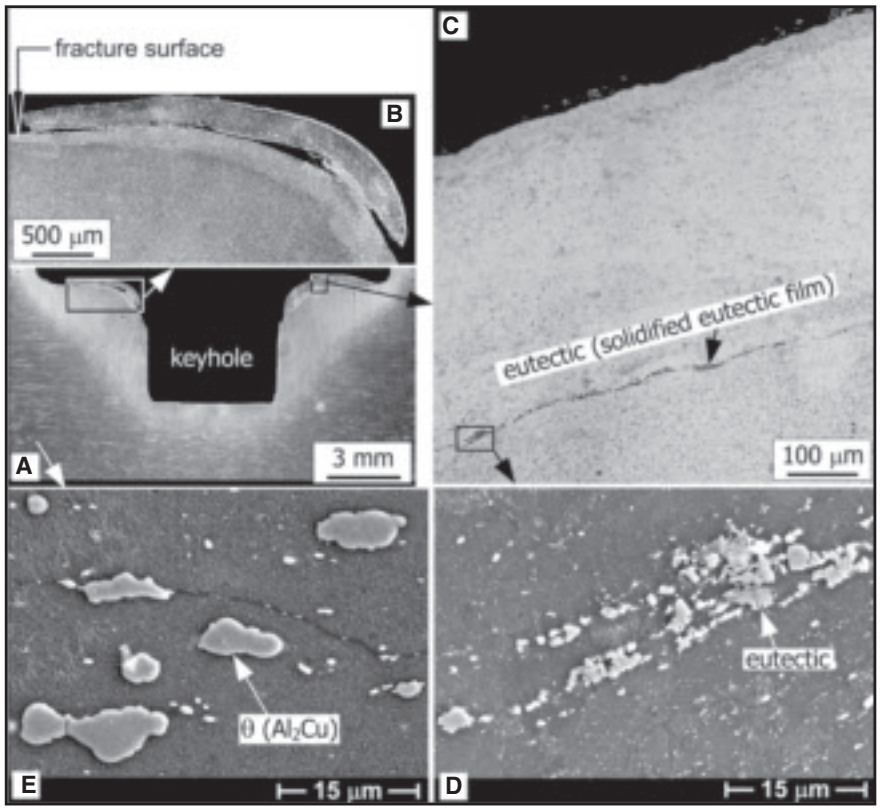

Fig. 13 — High concentration of eutectic particles suggesting presence of eutectic liquid film caused fracture. A — Vertical weld cross section of weld in Fig. 12; B — broken piece on fracture surface; C — string of eutectic particles at location corresponding to fracture surface in B; D — SEM image of eutectic particles in the string; E — SEM image of θ particles far away from weld.

mirror-like weld surface and the residue left on it by the material removed by the tool. Figure 11A is the same weld surface shown previously in Fig. 10B. This weld surface is mirror like not only on the top but also in the keyhole. The islands (light color) were the residue left on the weld surface by the material removed by the tool. Figure 11B is a SEM image of the vertical cross section of the weld showing the weld surface and a piece of the residue left on it, which can also be seen in Fig. 10D. The enlarged SEM image in Fig. 11C shows that the residue is rich in eutectic, about 26% as determined by the image analyzer software ImageJ V1.37 (Ref. 28). More importantly, a eutectic film is visible at the interface between the weld surface and the residue. The eutectic film and the material along the grain boundaries in the residue are composite-like eutectic ($\alpha + \theta$). Figure 11D shows both the composite-like eutectic ($\alpha + \theta$) and cracks along grain boundaries, and thus clear evidence of cracking in the stir zone.

The microstructural change from the residue to the weld was abrupt in terms of the grain structure and the eutectic content. There was no evidence of epitaxial growth of grains across the interface. The abrupt microstructural change from the residue to the weld across their interface and the nearly flat weld surface together suggest that during welding, the material stuck to and subsequently removed by the tool was perhaps rotating against the stationary material that stayed as the resultant weld — with a eutectic liquid film at the interface.

The presence of a eutectic film between the weld surface and the residue on it (Fig. 11C) suggests that during welding, a liquid eutectic film was present between the material stuck to and later removed by the tool and the material that stayed behind as the resultant weld. However, it is unclear how the eutectic liquid film formed. Perhaps, the material stuck to the tool was rotating and the rotating front was advancing as the tool penetrated deeper into the workpiece. This rotating and advancing front might have gradually collected the eutectic liquid ahead of it into a eutectic liquid film. The eutectic liquid can include the eutectic produced near the tool shoulder and the eutectic formed by θ particles.

As can be seen in Fig. 11B, both above and below the residue, a eutectic film is no longer visible on the weld surface. Had the vertical cross section of the weld surface missed the residue, the eutectic film would not have been observed. This explains why the liquid-film formation on a mirror-like surface has been difficult to confirm.

Transmission of Forces from Tool through Liquid Film

The liquated stir zone can still be subjected to both the tool torque during welding and the tool withdrawal force at the end of welding even when a eutectic liquid film is present at the interface between the material removed by the tool and the material that stays behind as the resultant weld. This is because the eutectic film is very thin and thus can effectively transmit the tool torque and lifting force. According to fluid me-

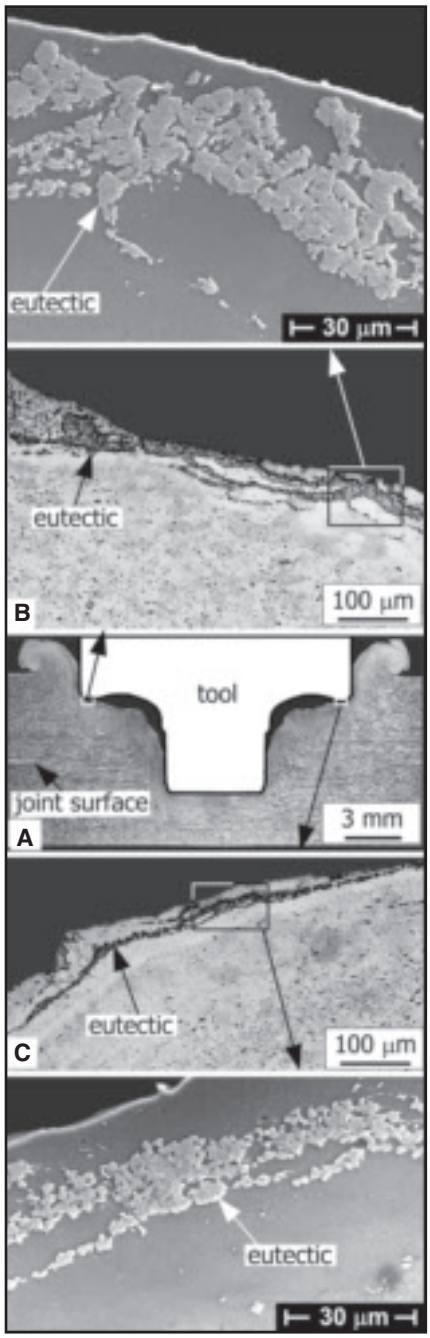

Fig. 14 — High concentrations of eutectic particles at outer edge of tool shoulder suggesting formation of liquid films at the tool edge during FSSW. A — Vertical cross section; B — optical micrograph and SEM image showing string of eutectic particles; C — similar to B.

chanics, the thinner the liquid between a rotating surface and a stationary one, the higher the shear stress under the same torque becomes (Ref. 29). Also, according to the hot tearing theory, the thinner a liquid film is between two solid surfaces, the greater a normal force it can transmit to separate them (Ref. 30). Thus, the presence of a eutectic liquid film at the interface during welding does not contradict the presence of cracks in the weld.

Mirror-Like Fracture Surface

A mirror-like fracture surface was observed in welds that fractured during welding. Figure 12A shows a weld made with the Lagun machine at 2000 rev/min. The SEM image in Fig. 12B shows that the top surface of the weld away from the fracture surface contained numerous microcracks along the circular tracks left by the rotating tool shoulder. On the contrary, the SEM image in Fig. 12C shows that the fracture surface appeared microscopically smooth. This explains why the fracture surface looked mirror like.

The mirror-like fracture surface suggests that the presence of a liquid film that was not continuous all (360 deg) around the tool during welding had caused fracture upon tool withdrawal. Where the liquid film was discontinuous or not fully developed, the material in contact with the tool was still bonded to the material underneath. Thus, only the material in contact with both the tool and the continuous portion of the liquid film broke off. Since the tool was still rotating at the full speed, the material broken off dragged along the surface of the remaining material and left marks on it, as can be seen in Fig. 12A.

High Concentrations of Eutectic Particles

The microstructure of the weld shown in Fig. 12A was examined by both optical and scanning electron microscopy. Referring to Fig. 12A, the weld was cut from about the 8 o'clock position (in order to include part of the mirror-like fracture surface and part of the broken top surface) through the axis to about the 2 o'clock position. Figure 13A is the resultant vertical cross section of the weld. Figure 13B shows a piece of broken top surface on the fracture surface.

A high concentration of eutectic particles was observed under the weld surface at a location corresponding to the location of the fracture surface. Figure 13C shows a string of particles below the top surface on the right along a curved path corresponding to the fracture surface on the left — Fig. 13B. The area where much more particles accumulated than elsewhere along the string is enlarged in the SEM image in Fig. 13D. These particles are similar to the θ (Al_2Cu) particles in the workpiece, though smaller. The SEM image in Fig. 13E shows the θ (Al_2Cu) particles in the workpiece in an area far away from the weld. EDS showed that both the particles along the string and the θ (Al_2Cu) particles in the workpiece had a composition of about Al-57Cu (by wt-%), which is close to the Al-53.5Cu composition of the θ phase according to the phase diagram — Fig. 6.

The high concentration of eutectic particles in Fig. 13C suggests the presence of a thin eutectic liquid film along the particles during welding. The location of these eutectic particles corresponds to that of the mirror-like fracture surface. These particles, as shown in Fig. 13D, are θ (Al_2Cu) particles. They are divorced eutectic that formed when the eutectic liquid film solidified. In Alloy 2219, liquid eutectic can solidify as a composite-like eutectic (θ + α). However, it can also solidify as a divorced eutectic, that is, it solidifies from upon the adjacent α matrix and results in a eutectic structure of θ surrounded by α. This is especially common when the liquid eutectic is small in size. Huang and Kou (Ref. 17) have observed divorced eutectic in the partially melted zone of gas metal arc welds of Alloy 2219, where liquation occurred during welding.

As a piece of background information, in the production of Alloy 2219, the composite-like eutectic (θ + α) formed during ingot casting became coarse θ (Al_2Cu) particles during heat treating, and during subsequent rolling they were broken up into smaller particles more or less lined up along the rolling direction, which is from left to right in Fig. 13E. As mentioned previously, the number and size of θ particles vary from place to place. In fact, there are more large θ particles in the area shown in Fig. 13E than the average.

Strings of eutectic particles were also observed near the weld surface at the outer edge of the shoulder. Figure 14A shows the vertical cross section of a weld made with the HAAS milling machine. The spot weld was made between two pieces of Alloy 2219 at 3000 rev/min. Much material was removed from the weld by the tool. Figure 14B and C show strings of divorced eutectic, that is, the θ particles, at the outer edge of the tool shoulder. These particles suggest that eutectic liquid films formed during FSSW. The films formed because of liquation induced by the friction heat generated at the shoulder edge during welding.

The formation of eutectic liquid films near the outer edge of the tool shoulder is likely to continue with the penetration of the shoulder into the workpiece during FSSW because, as shown in Figs. 8 and 14A, the outer edge of the shoulder is always in contact with the fresh material in the workpiece (instead of the liquated material that is subsequently removed). Perhaps these eutectic liquid films can contribute significantly to the formation of the liquid eutectic film at the interface between the material removed by the tool and the material that stays behind as the resultant weld.

Conclusions

The conclusions regarding the liquation tendency and the liquid-film formation in FSSW are as follows:

1. The augmented-torque testing proposed recently by the authors can be used to assess the liquation tendency in FSSW. For instance, under the same FSSW schedule, the liquation tendency increases in the order of 6061-T6 Al, 2219-T851 Al, and as-cast AZ91E Mg.

2. Under the same FSSW schedule, the torque and hence the heat input decrease in the order of 6061-T6 Al, 2219-T851 Al, and as-cast AZ91E Mg. This suggests that the increasing liquation tendency in the same order is not caused by the heat input but by the alloys themselves.

3. Liquation can limit the maximum torque to be reached in FSSW and cause the torque to fluctuate during FSSW. Under the same FSSW schedule, the maximum torque decreases in the order of 6061-T6 Al, 2219-T851 Al, and as-cast AZ91E Mg.

4. The method proposed recently by the authors based on both the phase diagram and the T-f_S curve can be used to explain the liquation tendency of an alloy. For instance, the content of the liquation-inducing constituent increases and the liquation temperature decreases in the order of 6061-T6 Al, 2219-T851 Al, and as-cast AZ91E Mg according to the Al-Cu phase diagram and the T-f_S curves of the alloys. This explains the increasing liquation tendency in the same order.

5. The extent of material removal by the tool in FSSW of 2219-T851 Al increases with increasing tool rotation speed. As the rotation speed increases, the material removal extends from under the shoulder to around the pin, which can reduce the joint strength significantly by reducing the bonding area.

6. The evidence of liquid-film formation observed in 2219-T851 Al in FSSW includes: 1) A thin eutectic film at the interface between the weld and the residue left on the weld surface by the material removed by the tool, 2) thin smooth eutectic films in the stir zone, 3) a mirror-like weld surface or fracture surface, and 4) a high concentration of eutectic particles in the stir zone at a location corresponding to the fracture surface.

7. Liquation during FSSW of 2219-T851 Al can cause material removal by the tool, erosion, or fracture at the weld surface, and cracking in the stir zone, either along smooth eutectic films or zigzagged grain boundaries.

Acknowledgments

This work was supported by National Science Foundation under Grant Nos. DMR-0098776 and DMR-0455484. The authors would like to thank 1) John F. Hinrichs of Friction Stir Link, Inc., Menomonee Falls, Wis., for suggesting the topic of liquation in FSSW for study; 2) Professor Thomas H. North of University of Toronto, Toronto, Canada, and his former graduate student Adrian P. Gerlich (now assistant professor, University of Alberta, Edmonton, Alberta, Canada) for sharing their publications on FSSW; and 3) Professor Frank Pfefferkorn of University of Wisconsin-Madison and his graduate student Axel Fehrenbacher for assistance in the torque and axial-force measurements.

References

1. Thomas, W. M., et al. Dec. 6, 1991. Friction stir butt welding. International Patent Application No. PCT/GB92, Patent Application No. 9125978.8.

2. Murr, L. E., Liu, G., and McClure, J. C. 1997. Dynamic recrystallization in friction-stir welding of aluminum alloy 1100. *Journal of Materials Science Letters* 16: 1801–1803.

3. Murr, L. E., Li, Y., Trillo, E. A., Nowak, B. M., and McClure, J. C. 1999. A comparative study of friction-stir welding of aluminum alloys. *Aluminum Transactions* 1: 141–154.

4. Cao, G., and Kou, S. 2005. Friction stir welding of 2219 aluminum: Behavior of θ (Al_2Cu) particles. *Welding Journal* 84(1): 1-s to 8-s.

5. Gerlich, A., Su, P., and North, T. H. 2005. Peak temperatures and microstructures in aluminum and magnesium alloy friction stir spot welds. *Science and Technology of Welding and Joining* 10(6): 647–652.

6. Yamamoto, M., Gerlich, A., North, T. H., and Shinozaki, K. 2007. Mechanism of cracking in AZ91 friction stir spot welds. *Science and Technology of Welding and Joining* 12(3): 208–216.

7. Yamamoto, M., Gerlich, A., North, T. H., and Shinozaki, K. 2007. Cracking in the stir zones of Mg-alloy friction stir spot welds. *Journal of Materials Science* 42: 7657–7666.

8. Gerlich, A., Yamamoto, M., and North, T. H. 2007. Local melting and cracking in Al 7075 and Al 2024-T3 friction stir spot welds. *Science and Technology of Welding and Joining*. In press.

9. Gerlich, A. P. 2007. Local melting and tool slippage during friction stir welding of aluminum alloys. PhD thesis, Department of Materials Science and Engineering, University of Toronto, Toronto, Ont., Canada.

10. Yang, Y. K., Dong, H., Cao, H., Chang, Y. A., and Kou, S. 2008. Liquation of Mg alloys in friction stir spot welding. *Welding Journal* 87(7): 167-s to 177-s.

11. Cao, G., and Kou, S. 2006. Predicting and reducing liquation-cracking susceptibility based on temperature vs. fraction solid. *Welding Journal* 85(1): 9-s to 18-s.

12. Huang, C., Cao, G., and Kou, S. 2004. Liquation cracking in partial-penetration aluminum welds: Assessing tendencies to liquate, crack and backfill. *Science and Technology of Welding and Joining* 9: 1–9.

13. Huang, C., and Kou, S. 2004. Liquation cracking in full-penetration Al-Cu welds. *Welding Journal* 83(2): 50-s to 58-s.

14. Huang, C., and Kou, S. 2004. Liquation cracking in full-penetration Al-Mg-Si welds. *Welding Journal* 83(4): 111-s to 122-s.

15. Huang, C., and Kou, S. 2002. Liquation mechanisms in multicomponent aluminum alloys during welding. *Welding Journal* 81(10): 211-s to 222-s.

16. Huang, C., and Kou, S. 2001. Partially melted zone in aluminum welds: Solute segregation and mechanical behavior. *Welding Journal* 80(1): 9-s to 17-s.

17. Huang, C., and Kou, S. 2000. Partially melted zone in aluminum welds — Liquation mechanism and directional solidification. *Welding Journal* 79(5): 113-s to 120-s.

18. Kou, S. 2003. *Welding Metallurgy*, 2nd ed. New York, N.Y.: John Wiley and Sons, pp. 303–339.

19. The Aluminum Association. 1982. *Aluminum Standards and Data*. Washington, D.C.: The Aluminum Association, p. 15.

20. Pew, J. W., Nelson, T. W., and Sorensen, C. D. 2007. Torque based weld power model for friction stir welding. *Science and Technology of Welding and Joining* 12: 341–347.

21. Pandat — Phase Diagram Calculation software package for Multicomponent Systems. 2001. CompuTherm LLC, Madison, Wis.

22. PanAluminium — Thermodynamic Database for Commercial Aluminum Alloys. 2001. CompuTherm LLC, Madison, Wis.

23. Ohno, M., Mirkovic, D., and Schmid-Fetzer, R. 2006. Liquidus and solidus temperature of Mg-rich Mg-Al-Mn-Zn alloys. *Acta Materialia* 54: 3883–3891.

24. American Society for Metals. 1986. *Binary Alloy Phase Diagrams vol. 1*. Metals Park, Ohio: American Society for Metals, p. 106.

25. Pepe, J. J., and Savage, W. F. 1967. Effects of constitutional liquation in 18-Ni maraging steel weldment. *Welding Journal* 46(9): 411-s to 422-s.

26. Pepe, J. J., and Savage, W. F. 1970. Weld heat-affected zone of the 18Ni maraging steels. *Welding Journal* 49(12): 545-s to 553-s.

27. Kou, S. 2003. *Welding Metallurgy*, 2nd ed. New York, N.Y.: John Wiley and Sons, pp. 303–339.

28. ImageJ. Dec. 28, 2006. Available online at the NIH Web site *http://rsb.info.nih.gov/ij/docs/index.html*.

29. Bird, R. B., Stewart, W. E., and Lightfoot, E. N. 1960. *Transport Phenomena*. New York, N.Y.: John Wiley, pp. 98–101.

30. Saveiko, V. N. 1960. Theory of hot tearing. *Liteinoe Proizvodstzo* 8: 453–456.